Int. J. Electrochem. Sci., 15 **(2020)** 1465 – 1473, doi: 10.20964/2020.02.57

International Journal of
ELECTROCHEMICAL
SCIENCE
www.electrochemsci.org

Short Communication

Hydrothermal Synthesis of MnO_2 with Different Morphological Characteristics as Electrode Material for High Electrochemical Performance Supercapacitors

Ying Zheng[1,*], *Xianfeng Zheng*[2]

[1] School of Vehicle Engineering, Xi'an Aeronautical University, Xi'an, 710165, China.
[2] Measuring and Testing Institute Under Xi'an Aerospace Corporation, Xi'an, 710100, China.
[*]E-mail: profzhengying@aliyun.com

Received: 2 October 2019 / *Accepted:* 10 December 2019 / *Published:* 31 December 2019

The morphology of the materials has a direct influence on the electrochemical performance of the electrode materials for the supercapacitors. Many works have been reported the improvement of electrochemical performance by designing different kinds of electrode materials for supercapacitors. However, the researchers have paid little attention about the influence of nanostructures of one material on the supercapacitors. Therefore, we developed morphology controlled MnO_2 nanostructures, including MnO_2 nanospheres (MN-NS) and MnO_2 nanocages (MN-NC), to modify the electrochemical performance of the supercapacitors. The electrochemical performance indicates that the as-prepared MN-NC electrodes exhibit higher specific capacity and superior cycle stability. This is ascribed to the hollow nanocages of MN-NC providing enough electrolyte to ensure the wettability of the whole electrode film.

Keywords: Supercapacitor, MnO_2, nanocages, nanostructures, Capacity, Energy density, New energy

1. INTRODUCTION

Energy storage and usage has become a regular topic for the researchers all over the world [1, 2]. According to the environment report, the traditional fuel could sustain the industry and life for two hundred years [3, 4, 5]. So, the shortage of energy storage is more and more evident in our daily life. Therefore, it is urgent to develop new energy storage systems, which could replace the traditional fuel, such as oil [6], gas [7] and goal [8]. During the past decades, scientists are fully devoted to design and develop various energy storage systems, including lithium-ion batteries [9], lithium-sulfur batteries [10], sodium metal batteries [11] and supercapacitors [12]. Among these systems, supercapacitors are one of the most promising candidates to replace the traditional fuel. Supercapacitors have high energy density and high power density at the same time, which is more excellent than the traditional lithium-

ion batteries [13, 14].

However, the electrochemical performance is limited due to the electrode materials for the supercapacitors. As we all know, the kind of electrode materials will cause significant effect on the electrochemical performance of supercapacitors. To overcome the problems, many kinds of electrode materials are prepared and used for supercapacitors [15]. Xu et al used carbon-based electrode materials to prepare supercapacitors [16]. The as-prepared supercapacitors showed 4 Wh Kg^{-1} at 564 W Kg^{-1}. Besides, various carbon materials were reported to employ as electrode materials for the supercapacitors, such as graphene [17], hollow carbon spheres [18], carbon nanotube [19] and carbon nanofiber [20]. All of these carbon-based materials exhibit superior electrochemical performance. Moreover, metal oxides are recognized as suitable electrode materials for the supercapacitors. However, great amounts of works pay their attentions on the design of kinds of materials. They failed to realize the morphology of electrode could have an effect on the electrochemical performance.

In this paper, we studied the influence of electrode material morphology on the electrochemical performance. We firstly prepared different morphology of MnO_2 materials by controlling the reaction time via hydrothermal method. The electrochemical results indicate that the as-prepared MnO_2 nanocages show higher capacity and energy density than the MnO_2 nanospheres. The superior electrochemical performance is attributed to the unique nanocage structure, which could ensure the wettability and promote the transport of the electronics.

2. EXPERIMENTAL

2.1. Preparation of MN-NS and MN-CN

For the preparation of the MnO_2 samples, a hydrothermal method was applied to prepare different morphologies of the MnO_2 materials. Briefly, 2.6 g $Mn(NO_3)_2$ was added into 60 ml ethanol under stirring for 30 min. After that, 1.3 g KMnO4 was dissolved into the above solution. Finally, the mixture was transferred into sealed stainless steel vessel and heated at 110℃ for 2 h and 120℃ for 3 h, respectively. The resultant products were washed by using distilled water and ethanol three times, dried at 80 ℃ for 30 min. As a result, different morphologies of the MnO_2 materials are prepared, MN-NS and MN-CN, respectively.

2.2. Materials Characterization

SEM and TEM images were obtained by using scanning electron microscpoy (Nova Nano450) and transmission electron microscopy (Tecnai G2F30). N_2 adsorption/desorption isotherms were measured on a Micromeritics ASAP2020 analyzer. XRD pattern was obtained by using X-ray diffractometer with Cu target on a Bruker VERTEX 70 research spectrometer. XPS was carried out on a GENESIS energy spectrometer.

2.3. Electrochemical Measurements

All electrochemical measurements were conducted with an electrochemistry station (CHI660E), including CV curves and discharge and charge profiles. The detailed steps are as following: First, the as-prepared MN-NS and MN-CN samples are mixed with super carbon as conductive agent and polytetrafluoroethylene as the binder by the weight ratio of 90:5:5. Then, the above mixture was coated onto the nickel foam current collector and dried at 80 °C for 24 h. The electrochemical performances are conducted by using three-electrode system in 8 M KOH aqueous electrolyte. These were used as working electrode, reference electrode and counter electrode, respectively.

3. RESULTS AND DISCUSSION

Figure 1 shows the morphology of the as-prepared materials. As shown in Figure 1a and b, the as-prepared MnO_2 materials shows nanospheres structure. It can be seen that the MnO_2 nanospheres are uniformly dispersed with a dimeter of 100 nm. With the increase of the heating temperature, the morphology of MnO_2 varies from nanospheres to nanocages structure. The morphology has direct relationship with the reaction temperature.

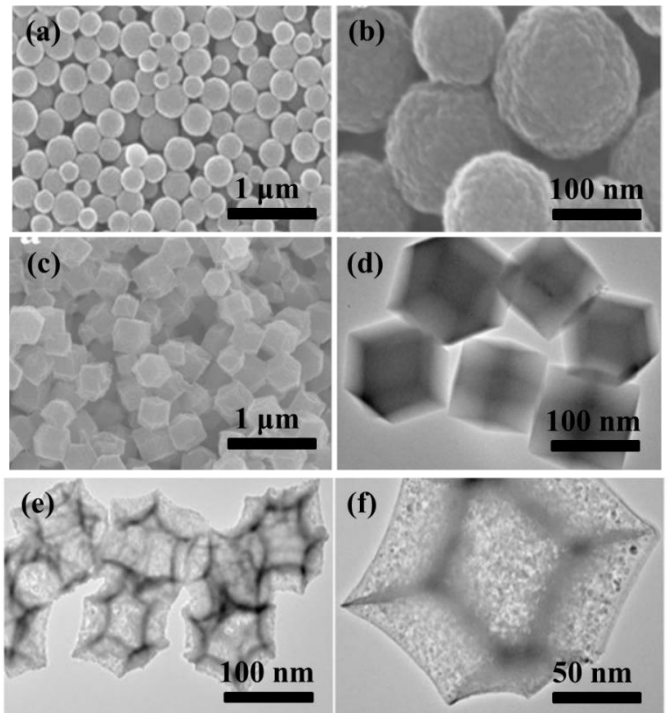

Figure 1. (a) and (b) SEM images of MnO_2 nanospheres. (c) and (d) SEM images of MnO_2 nanocages. (e) and (f) TEM images of MnO_2 nanocages.

As shown in Figure 1c and d, the as-prepared MnO_2 materials display nanocage structure, which demonstrates nano cubic shape. This unique structure is related to the reaction time and

temperature during the preparation of MnO_2 materials. To further observe the internal structure of MN-CN, TEM images were displayed in Figure 1e and f. It can be clearly observed that the as-prepared MN-CN exhibits hollow cubic structure. Besides, the dimeter of the MN-CN locates between 100-120 nm. The hollow cubic structure could keep its structure stability during the electrochemical process.

Figure 2a is the XRD pattern of the MN-NS and MN-CN. The as-prepared MN-NS and MN-CN display the same diffraction peaks. This is consistent with other reports about the XRD of MnO_2. Typically, the as-prepared MN-NS and MN-CN shows peaks at 25°, 37° and 46°, which is ascribed to the crystal plane of (110), (111), and (112), respectively. This indicates that the samples are of high purity. As a result, the high purity could ensure the sufficient capacity contribution during the discharging and charging process. The high purity could ensure the sufficient capacity release and promote the total electrochemical reaction during the discharge and charge process. To investigate the chemical valance in the MnO_2 samples, X-ray photoelectron spectroscopy was conducted for MN-NC. As shown in Figure 2b, for the Mn 2p, there are two main peaks at 833.1eV and 845.6 eV, respectively. These peaks are corresponding to the Mn $2p_{1/2}$ and Mn $2p_{3/2}$, confirming the successful preparation of MN-CN materials [21]. The typical peaks could confirm the successful preparation of the two different kinds of MnO2 materials.

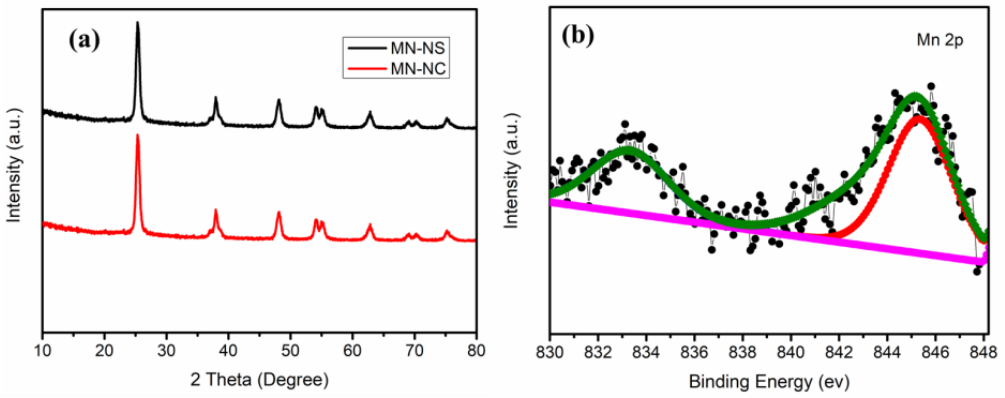

Figure 2. (a) XRD patterns of the MnO_2 nanospheres and MnO_2 nanocages. (b) X-ray photoelectron spectroscopy of Mn 2p for the MN-NC.

N_2 adsorption and desorption isotherms of the MN-NS and MN-CN materials were tested to investigate the specific surface of the samples. As shown in Figure 3, the MN-CN shows typical IV isotherms, which indicates that the MN-CN has mesoporous structure. Besides, the specific surface of the MN-CN sample is as high as 86 m^2/g, which is higher than the MN-NS materials (53 m^2/g). This high specific surface area could provide enough active reaction space for the electrochemical reaction. Besides, the abundant mesorporous structure is beneficial for the electrolyte storage. Therefore, the whole electrode film is high wettability during the electrochemical reaction. This result is related to the superior electrochemical performance with long cycle stability and high specific capacity. This is attributed the presence of unique hollow cubic structure.

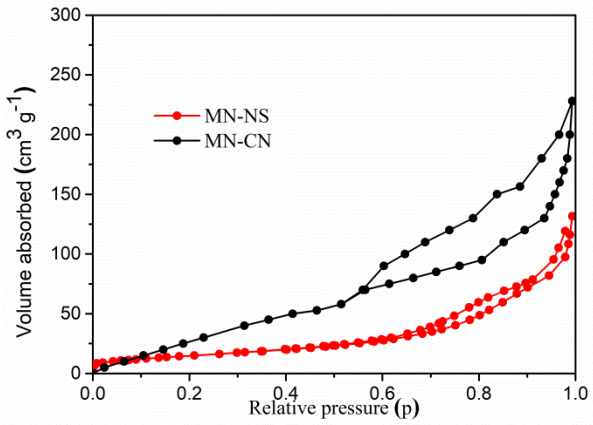

Figure 3. N_2 adsorption and desorption isotherms of the MN-NS and MN-CN materials.

To study the electrochemical performance of the as-prepared MN-NS and MN-CN samples, various electrochemical measurements were conducted for the MN-NS and MN-CN electrodes. As shown in Figure 4a, it shows the CV curves of the MN-NS electrode at various scan rates from 5 mV/s to 100 mV/s. The CV curves of MN-NS exhibit typical capacitor behavior. Besides, the CV area becomes larger with the increase of the scan rate during the CV test. Figure 4b displays the constant discharge and charge profiles at different current densities from 0.1 A/g to 10 A/g. When the current density is 0.1 A/g, the DC profile of MN-NS electrode has a slope with a low ratio, which is consistent with the CV curves at low scan rate.

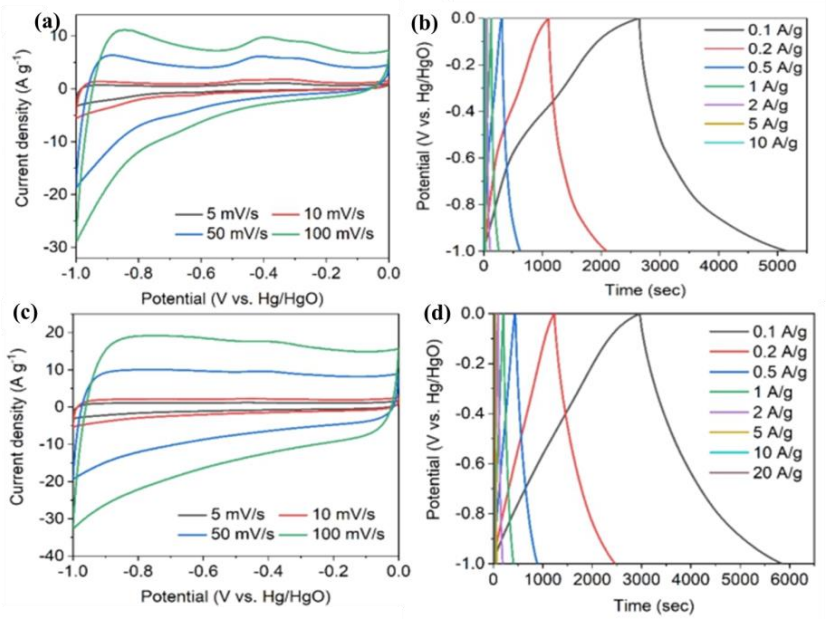

Figure 4. (a) and (c) CV curves of the MN-NS and MN-CN electrodes. (b) and (d) The constant discharge and charge profiles of the MN-NS and MN-CN electrodes at different current densities.

For the MN-CN electrode, the CV curves (Figure 4c) clearly shows a larger area than that of the MN-NS electrode. This phenomenon is caused due to the different morphologies of MN-CN,

which has unique cubic structure. This cubic structure could provide enough space for the storage of electrolyte [22]. As a result, the CV curves of MN-CN shows larger area than the MN-NS electrode. Figure 4d is the DC profiles of MN-CN electrode. Evidently, it can be seen that the MN-CN electrode possesses higher specific capacity at various current densities from 0.1 A/g to 10 A/g. Even at the high current density of 20 A/g, the MN-CN electrode can still remain normal discharge and charge process.

Furthermore, the long term cycle stability of the MN-NS and MN-CN electrode in the supercapacitors are compared, as shown in Figure 5a and b. First, for the MN-NS electrode, it shows initial specific capacity of 121 F/g at 0.1 A/g with capacity retention of nearly 83% after 500 cycles. The as-prepared MN-CN electrode shows initial specific capacity as high as 278 F/g, which is much higher than the MN-NS electrode. More importantly, the specific capacity of MN-CN electrode still remains at nearly 200 F/g after 2000 cycles at 0.1 A/g. In a word, the MN-CN electrode shows long cycle stability, which is attributed the unique nanocage structure. This structure is steady during electrochemical process. However, the as-prepared MN-NS electrode is easier to collapse than the MN-CN electrode. As a result, the MN-NS electrode suffers from severe capacity fade with the increase of the cycle numbers. Because the MN-NS failed to restrain the volume change during the electrochemical process [23, 24]. The structure will be destroyed when the cycle numbers are increased. As for the MN-CN electrode, the perfect nanocage structure could keep superior structure stability during the electrochemical reaction [25].

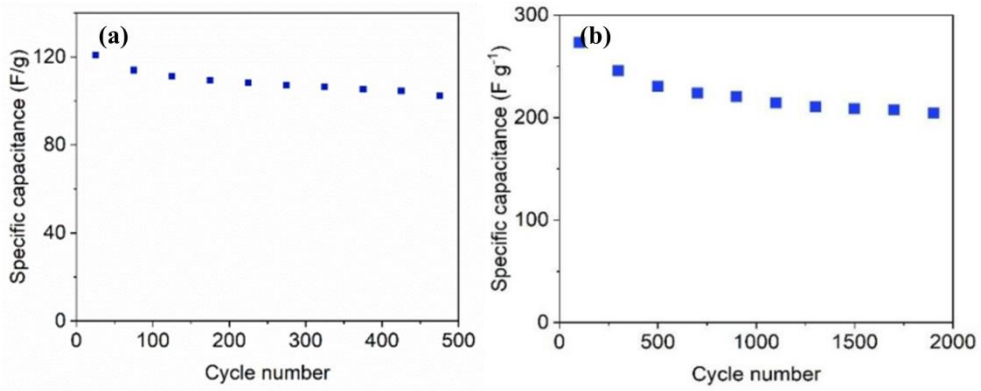

Figure 5. (a) and (b) Comparison of long cycle stability for MN-NS and MN-CN electrodes at the current density of 0.5 A g^{-1}, respectively.

Rate performance is key index for the electrochemical performance of the supercapacitors. To further verify the superior electrochemical performance of MN-CN electrode, the rate performance was tested. As shown in Figure 6a, it can be seen that the specific capacities of MN-CN electrode are 152 F/g, 126 F/g and 118 F/g at the current density of 0.5 A/g , 1 A/g and 2 A/g, respectively. Therefore, the MN-CN electrode exhibits high rate performance at various rates even at 2 A/g. High energy density and power density are important for the electrode materials in the supercapacitors. Figure 6b shows the ragone plot for the supercapacitor of MN-CN electrode. According to the energy density equation, it can be obtained that the MN-CN electrode shows high energy density of 38 Wh/kg

at power density of 486 W/kg. In all, the as-prepared MN-CN electrode shows excellent rate capability and high power density and energy density at the same time. These superior electrochemical performances are ascribed to the unique nanocage structure, which are beneficial for the structure stability and easy electronic transport.

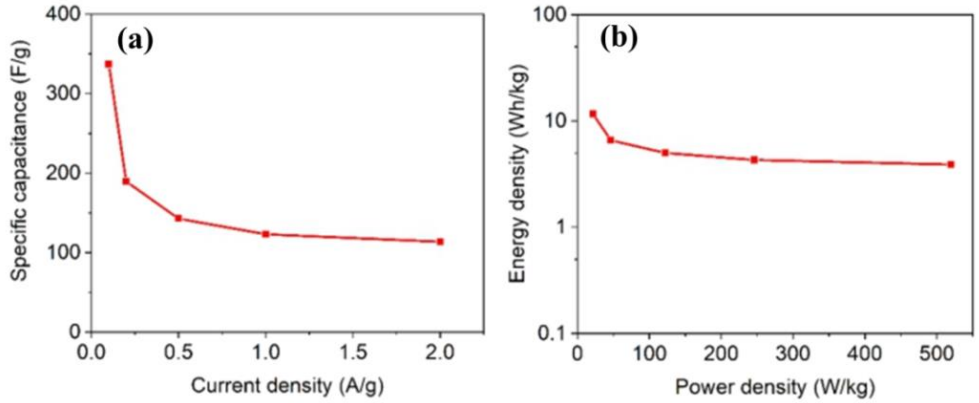

Figure 6. (a) The capacity variation with the increase of the current density from 0 to 2.0 A/g for MN-CN electrode. b) Ragone plot for MN-CN electrode full supercapacitor.

To investigate the superior electrochemical performance of the MN-CN electrode materials, a table was made for comparing the electrochemical performance of the various electrode materials for the supercapacitors. As listed in Table1, it can be seen that the as-prepared MN-CN electrode shows more superior cycle stability, which is much higher than the reported electrode materials for the supercapacitors. Therefore, the as-prepared MN-CN electrode materials are a promising electrode materials for the employment of supercapacitors. The superior electrochemical performance is attributed to the unique nanocage structure, which could keep structure stability during the electrochemical process.

Table 1. Comparison of the MN-CN electrode with other reported electrode materials for the supercapacitors.

Electrode	Capacity Retention	Ref
CO-SO	72% (500 cycles)	26
CO/MN	82% (500 cycles)	27
Mn@Co_3O_4	74% (500 cycles)	28
MN-CN	83% (500 cycles)	This Work

4. CONCLUSIONS

In summary, different morphologies MnO_2 materials are prepared and designed as electrode materials for the supercapacitors. Through electrochemical tests, it can be obtained that the as-prepared MN-CN shows higher capacity and energy density than the MN-NS. As for the reason, the superior electrochemical performance is related to the unique nanostructure of MN-NC, which could restore enough electrolytes and promote the transport of electronics. Therefore, our work may provide a new method to prepare high-performance supercapacitor electrode materials.

ACKNOWLEDGEMENT
This work is financial supported by Xi'an Aeronautical University School Research Fund Project: Simulation analysis of chassis performance of pure electric vehicle and design of experimental platform (2018KY1225).

References

1. B. S. Yin, S. W. Zhang, K. Ke and Z. B. Wang, *J. Alloy Compd*., 805 (2019) 1044.
2. W. Xiong, K. Hu, Z. Li, Y. X. Jiang, Z. G. Li, Z. Li and X. W. Wang, *Nano Energy*, 66 (2019) 104149.
3. J. L. Yu, J. Zhou, P. P. Yao, J. T. Huang, W. C. Sun, C. Z. Zhu and J. Xu, *J. Power Sources*, 440 (2019) 227150.
4. J. J. Cao, Q. F. Mei, R. L. Wu and W. Wang, *Electrochim. Acta*, 321 (2019) 134711.
5. T. Das and B. Verma, *J. Energy Storage*, 26 (2019) 100975.
6. L. J. Deng, Z. Y. Ma, Z. H. Liu and G. Fan, *J. Alloy Compd*., 812 (2020) 152087.
7. Z. F. Wu, K. W. He, Y. Z. Wu, J. Mao, Z. C. Yang, Y. T. Xu, C. H. Yuan, B. R. Zeng and L. Z. Dai, *J. Power Sources*, 442 (2019) 227215.
8. H. C. Lee, G. M. Lee, J. Y. Yun, K. Y. Keum, S. Y. Hong, C. H. Song, J. W. Kim, J. H. Lee, S. Y. Oh, D. S. Kim, M. S. Kim and J. S. Ha, *Chem. Eng. J*., 366 (2019) 62.
9. L. J. Deng, Z. Y Ma, Z. H. Liu and G. Fan, *J. Alloy Compd*., 812 (2020) 152087.
10. Y. Y. Zhang, J. J. He, Z. Gao and X. D. Li, *Nano Energy*, 65 (2019) 104045.
11. E. Cevik, S. T. Gunday, S. Akhtar and A. Bozkurt, *Int. J. Hydrogen Energy*, 44 (2019) 16099.
12. L. Liu, H. M. Yu, A. Liu, Y. H. Xu, B. Feng, F. Q. Yang, P. X. Zhang, J. Wang, Q. Deng, Z. L. Zeng and S. G. Deng, *Electrochim. Acta*, 327 (2019) 134970.
13. H. L Wang, D. J. Wu and J. B. Zhou, *J. Alloy Compd*., 811 (2019) 152073.
14. J. J. Han, Q. Li, C. Peng, N. Shu, F. Pan, J. Q. Wang and Y. W. Zhu, *Appl. Surf. Sci*., 502 (2020) 144191.
15. J. M. Baptista, J. S. Sagu, U. W. K and K. Lobato, *Chem. Eng. J*., 374 (2019) 1153.
16. Z. Y. Zhao, T. Shen, Z. H. Liu, Q. S. Zhong and Y. J. Qin, *J. Alloy Compd*., 812 (2020) 152124.
17. L. S. Xu, H. B. Wang, J. M. Gao and X. J. Jin, *J. Alloy Compd*., 809 (2019) 151802.
18. X. H. Tang, B. W. Zhang, Y. H. Lui and S. Hu, *J. Energy. Storage*, 25 (2019) 100897.
19. L. Wan, P. Song, J. X. Liu, D. Q. Chen, R. Xiao, Y. Zhang, J. Chen, M. J. Xie and C. Du, *J. Power Sources*, 438 (2019) 227013.
20. J. Wu, X. P. Zhang, F. X. Wei, Y. W. Sui and J. Q. Qi, *Mater. Lett*., 258 (2020) 126761.
21. D. K. Nguyen, I. M. Schepisi and F. Z. Amir, *Chem. Eng. J*., 378 (2019) 122150.
22. J. Bhagwan, S. K. Hussain and J. S. Yu, *J. Alloy Compd*., 815 (2020) 152456.
23. G. F. Zhang, P. Qin and J. M. Song, *Appl. Surf. Sci*., 493 (2019) 55.
24. Q. F. Wu, Y. H. Zhao, J. Yu, D. L. Song, R. R. Chen, Q. Liu, R. M. Li and M. Q. Fan, *Int. J. Hrdrogen Energy*, 44 (2019) 31780.
25. C. Liu, A. M. Gao, F. Y. Yi, D. Shu, H. Yi, X. P. Zhou, J. N. Hao, C. He and Z. H. Zhu,

Electrochim. Acta, 326 (2019) 134965.
26. Z. H. Wang, Y. Long, D. Cao, D. M. Han and F. B, Gu, *Electrochim. Acta*, 307 (2019) 341.
27. G. Liu, C. X. Kang, J. Fang, L. K. Fu, H. H. Zhou and Q. M. Liu, *J. Power Sources*, 431 (2019) 48.
28. H. Y. Chen, J. P. Wang, F. Liao, X. R. Han, Y. F. Zhang, C. J. Xu and L. Gao, *Ceram. Int*., 45 (2019) 11876.